Syracuse University

SURFACE

Physics College of Arts and Sciences

2-6-2008

Plasticity in Current-Driven Vortex Lattices

Panayotis Benetatos
Syracuse University

M. Cristina Marchetti
Syracuse University

Follow this and additional works at: https://surface.syr.edu/phy

 Part of the Physics Commons

Recommended Citation

arXiv:cond-mat/10110237v1

This Article is brought to you for free and open access by the College of Arts and Sciences at SURFACE. It has been accepted for inclusion in Physics by an authorized administrator of SURFACE. For more information, please contact surface@syr.edu.

arXiv:cond-mat/0110237v1 [cond-mat.supr-con] 11 Oct 2001

Plasticity in current-driven vortex lattices

Panayotis Benetatos
Hahn-Meitner-Institut, Abteilung Theoretische Physik (SF5), Glienicker Str. 100, D-14109, Berlin, Germany

M. Cristina Marchetti
Physics Department, Syracuse University, Syracuse, NY 13244, USA
(February 6, 2008)

We present a theoretical analysis of recent experiments on current-driven vortex dynamics in the Corbino disk geometry. This geometry introduces controlled spatial gradients in the driving force and allows the study of the onset of plasticity and tearing in clean vortex lattices. We describe plastic slip in terms of the stress-driven unbinding of dislocation pairs, which in turn contribute to the relaxation of the shear, yielding a nonlinear response. The steady state density of free dislocations induced by the applied stress is calculated as a function of the applied current and temperature. A criterion for the onset of plasticity at a radial location r in the disk yields a temperature-dependent critical current that is in qualitative agreement with experiments.

I. INTRODUCTION

In the mixed state of type-II superconductors the magnetic field is concentrated in an array of flexible flux bundles that, much like ordinary matter, can form crystalline, liquid and glassy phases.[1,2] In clean systems the vortex solid melts into a flux liquid via a first order phase transition.[1] If the barriers to vortex line crossing are high, a rapidly cooled vortex liquid can bypass the crystal phase and get trapped in a metastable polymer-like glass phase, much like ordinary window glass.[3] The diversity of vortex structures is further increased by pinning from material disorder, which leads to a variety of novel glasses.[4,5]

Of particular interest is the *dynamics* of the vortex array in the various phases and in the proximity of a phase transition. In the liquid phase the vortex array flows yielding a linear resistivity. In the presence of large scale spatial inhomogeneities, the liquid flow can be highly nonlocal due to interactions and entanglement.[6,7] The correlation length controlling the spatial nonlocality of the flow grows with the liquid shear viscosity, which becomes large as the liquid freezes. At a continuous liquid-glass transition this correlation length diverges with a universal critical exponent.[8] In general, probing velocity correlations in driven vortex arrays yields information on vortex dynamics within a given phase, as well as on the nature of the phase transitions connecting the various phases.

As for ordinary matter, the shear rigidity of the vortex array can be probed by forcing the vortices to flow in confined geometries obtained by engineering suitable artificial pinning structures, as discussed for instance in Ref. 8. Large scale spatial inhomogeneities can also be introduced in the flow, even in the absence of pinning, by applying a driving force with controlled spatial gradients, as done recently by the Argonne group using the Corbino disk geometry sketched in Fig. 1.[9–11] In the Corbino disk a radial driving current, I, yields a spatially inhomogeneous Lorentz force that decreases as $\sim 1/r$, with r the distance from the center of the disk. For small applied currents, the local shear stresses are negligible and the vortex array moves as a rigid body. Larger currents (or even vanishingly small currents in a glassy solid) result in a strong spatially inhomogeneous stress, $\sigma(r, I)$. The solid "breaks up" in concentric annular regions flowing at different velocity and the response is highly nonlinear.[10] The voltage profiles measured experimentally by placing a series of voltage taps in the radial direction (see Fig. 1) reflect the different dynamical correlation lengths in the fluid, plastic and elastic regimes. In a given experiment, shear-induced plastic slip is observed to occur at different values of the applied current in different regions of the sample. This is a direct consequence of the controlled spatial inhomogeneity of the shear stress.

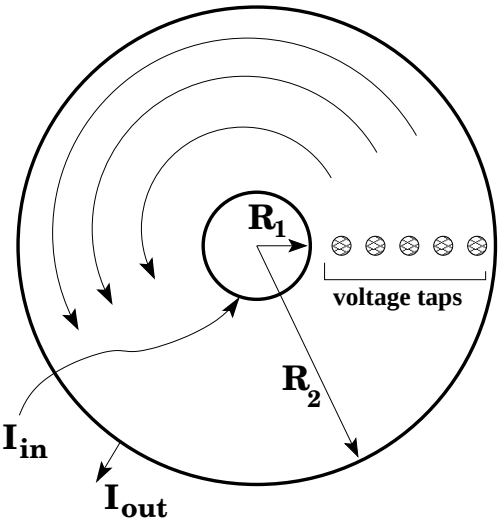

FIG. 1. The Corbino disk geometry. The external magnetic field is out of the page. The electrical current flows radially from the inner circumference to the outer rim of the disk. The radial current density gives rise to a Lorentz force which causes the vortices to moves in circular orbits around the disk, without crossing the sample edges.

Slippage occurs first in the inner region of the disk where the Lorentz force is largest, and propagates to the outer regions as the current is increased. In this regime of plastic response the dynamical correlation length controlling velocity inhomogeneities can be identified with the separation between free dislocations that are continuously created and annihilated by the strong local shear stresses.

In this paper, we present a theoretical analysis of these experiments. A preliminary account of part of this work was presented in Ref. 12. We describe the onset of plasticity in the driven vortex solid as a nonlinear effect due to the stress-induced proliferation of unbound dislocations. The static shear stress from the applied current yields a Peach-Koehler force that pulls apart neutral, bound dislocation pairs present in the lattice in equilibrium. As a result, a finite density, $n_f(\sigma, T)$, of free dislocations is generated in the solid. Such unbound dislocations can then contribute to the relaxation of the shear, resulting in a highly nonlinear response to the applied current. This mechanism for nonlinear shear relaxation has been studied before in the context of superfluid films[13], $2D$ solids[14,15] and smectic liquid crystal films[16]. In all this cases, the response to a spatially inhomogeneous shear was considered. Here we adapt this work to the case where the external shear is spatially inhomogeneous, but still slowly varying on the length scales of interest.

Although this paper deals specifically with the onset of plasticity in vortex lattices in the Corbino disk geometry, the methods and results presented have a more general interest. In particular, the Langevin and Fokker-Planck descriptions of dislocation dynamics in a spatially-inhomogeneous stress field can be used to describe nonlinear shear relaxation in other systems and geometries. Our work is for instance relevant to the defect dynamics in two-dimensional colloidal crystals, where individual point defects can be created and manipulated with optical tweezers.[17,18] Although only vacancies and interstitials have been considered so far, 2d colloids, where direct real space and time imaging of defects is possible, may be especially suitable for studying in details the dynamics of dislocations in the presence of external stresses.

We begin in Section II with a brief review of the Corbino disk geometry and of the qualitatively different response of a vortex liquid and a vortex solid to an applied radial current. In the vortex solid, static elastic deformations yield a local shear stress $\sigma(r, I)$, which, for the case of free boundary conditions, decreases as $\sim 1/r^2$. This stress can break bound dislocation pairs present in the solid in equilibrium, as shown in sections III and IV. For a finite external stress, the total interaction energy of a neutral dislocation pair exhibits a saddle point with a finite barrier at a value $x_c \sim 1/\sigma(r)$ of the pair separation. At zero temperature, the pair unbinds when the stress is large enough that $x_c(\sigma) \sim a_0$. At finite temperature unbinding takes place when the pair escapes via thermal activation over the barrier. Using Langevin and Fokker-Planck descriptions of the dynamics of bound pairs, we evaluate the rate of thermal escape and use this to estimate the density of free dislocation, $n_f(\sigma, T)$. The onset of plasticity is then identified with the proliferation of unbound dislocations. For free boundary conditions (which are appropriate for the Argonne experiments), the applied stress is largest near the center of the disk and, for a fixed current I, dislocations unbind first near the inner rim. We can then evaluate the critical current $I_{\rm pl}(r, T)$ where the onset of plastic slip occurs as a function of temperature T and of the radial distance from the center, with the result

$$I_{\rm pl}(r, T) = \frac{I_0(T)}{1 + A/r^2} \ , \tag{1.1}$$

with $A = 2R_1^2 R_2^2 \ln(R_2/R_1)/(R_2^2 - R_1^2)$ a geometrical factor. The characteristic current scale $I_0(T) = 4cc_{66}t/B_0 \exp[-b/(T_M - T)^{1/2}]$ is the current where shear induced proliferation of dislocations occurs across the entire sample, with T_M the Kosterlitz-Thouless melting temperature and b a numerical constant.[19] As observed in experiments, for fixed T, the current $I_{\rm pl}$ increases away from the center of the disk. Conversely, for fixed r, it is strongly temperature dependent and it decreases as the melting point T_M is approached from below.

II. THE CORBINO DISK GEOMETRY

The Corbino disk geometry was used recently by the Argonne group to introduce controlled spatial inhomogeneities in driven vortex arrays and study the onset of plasticity in clean samples, near the first order melting transition.[10] The same geometry has been used before to minimize edge effects[20] and also to study the Hall effect in type-I superconductors[21].

The Corbino disk is an annular superconducting slab placed in a magnetic field parallel to its axis (chosen here as the $\hat{\mathbf{z}}$ direction), as shown in Fig. I. A current I is injected at the center of the disk and removed at the outer boundary, creating a radial current density,

$$\mathbf{J}(r) = \frac{I}{2\pi r t} \ \hat{\mathbf{r}} \ , \tag{2.1}$$

where r is the radial distance from the center and t the thickness of the disk. With the magnetic field applied along the disk axis, the Lorentz force density on the vortices is azimuthal, with

$$\mathbf{f}_L(r) = \frac{1}{c} B_0 J(r) \hat{\boldsymbol{\phi}} \ , \tag{2.2}$$

and drives the vortices to move in circular orbits around the disk, without crossing the sample edges. Here, $B_0 = n_0 \phi_0$ is the average magnetic induction in the sample and $\hat{\boldsymbol{\phi}} = \hat{\mathbf{z}} \times \hat{\mathbf{r}}$ is the unit vector in the tangential direction. In this geometry, the driving force is spatially inhomogeneous and stronger near the center of the disk,

falling off as $\sim 1/r$. It naturally yields spatially inhomogeneous distortions of the vortex array that can be probed by placing a series of voltage taps in the radial direction. As described below, the spatial dependence of the voltage profile in this geometry is qualitatively different in the vortex liquid and solid phases and provides a natural way to study the onset of plasticity.

As described in Ref. 10, in the liquid state, vortex motion is governed by the hydrodynamic equation for the vortex flow velocity $\mathbf{v}$,[6,22]

$$-\gamma\mathbf{v} + \eta\nabla_\perp^2\mathbf{v} = -\mathbf{f}_L \ , \tag{2.3}$$

where $\gamma(T,H)$ is the friction and $\eta(T,H)$ the shear viscosity of the vortex liquid. The flow profile can be found by solving Eq. (2.3) with suitable boundary conditions.[12] The electric field induced by the vortex motion is then obtained from

$$\mathbf{E} = \frac{1}{c}\mathbf{B}\times\mathbf{v} \ . \tag{2.4}$$

If the radial width of the disk is much larger than the viscous penetration length, $\delta = \sqrt{\eta/\gamma}$, the effect of the boundaries is negligible and the velocity profile simply follows the force profile, with $\mathbf{v} = \mathbf{f}_L/\gamma$, i.e., $v \sim 1/r$. The voltage drop between the n-th and the $n+1$-th electrodes is then given by

$$V_{n,n+1} = \int_{R_n}^{R_{n+1}} E(r)dr = \frac{B_0^2 I}{\gamma c^2 2\pi t}\ln\left(\frac{R_{n+1}}{R_n}\right) . \tag{2.5}$$

where R_n is the radial location of the n-th electrode. This logarithmic scaling of the voltage characterizes fluid flow, with neglible spatial inhomogeneities caused by viscous effects at the boundaries.

In contrast, a vortex lattice with a finite shear modulus rotates as a rigid body due to the azimuthal applied force, provided the shear stresses due to the local force gradients are not too strong. This rigid body rotation yields a local velocity that scales as $\sim r$, with

$$V_{n,n+1} = \int_{R_n}^{R_{n+1}} E(r)dr = \frac{B_0\omega}{2c}\left(R_{n+1}^2 - R_n^2\right) , \tag{2.6}$$

where ω is the angular velocity of rotation of the vortex lattice, given by

$$\omega = \frac{B_0 I}{\pi c\gamma(R_2 - R_1)}\frac{1}{R_2^2 + R_1^2} \ , \tag{2.7}$$

with R_1 and R_2 the inner and outer radii of the disk, respectively. Above a certain value of the applied current, the local shear stresses become strong enough to break the lattice bonds, or generate unbound dislocations. In this regime, one obtains a plastic response where the lattice "breaks" into two or more concentric annular sections rotating at different angular velocities and slipping past each other due to the continuous generation and recombination of topological defects. Such a plastic response is evident in the experiments by the Argonne group.[10]

The spatial dependence of the Lorentz force makes it possible for all of the types of reponse mentioned above to coexist at a given value of the applied current. Near the inner radius of the disk the shear stress is very large and the vortex array flows like a liquid, with a logarithmic scaling of the voltage drop with the contact positions. In the middle of the disk the motion is plastic, with dislocations continuously being created and annihilated. Near the outer radius the shear stress is very small and the vortex array rotates as a rigid body. Evidence for the coexistence of these behaviors was obtained in Ref. 10 by measuring the potential drops across successive pairs of electrodes.

In this article, we describe the onset of plasticity in the driven vortex solid as a nonlinear effect due to the stress-induced proliferation of unbound dislocations. The spatially inhomogeneous Lorentz force gives rise to elastic deformations of the vortex lattice described by the solution of the equation

$$\mathbf{f}_{\rm el} + \mathbf{f}_L(r) = 0 \ , \tag{2.8}$$

where $\mathbf{f}_{\rm el}$ is the elastic force density, given by,

$$f_{{\rm el},i} = \partial_j\sigma_{ij} \ , \tag{2.9}$$

with σ_{ij} the stress tensor,

$$\sigma_{ij} = 2c_{66}u_{ij} + (c_{11} - c_{66})\delta_{ij}u_{ll} \ , \tag{2.10}$$

and $u_{ij} = (\partial_j u_i + \partial_i u_j)/2$ the symmetrized strain tensor. Elastic deformations are described in terms of the two-dimensional displacement field, $\mathbf{u}$, and c_{66} and c_{11} are the shear and compressional moduli of the vortex lattice, respectively. Since dense vortex arrays are practically incompressible ($c_{11} >> c_{66}$), Eq. (2.8) becomes simply

$$c_{66}\nabla_\perp^2\mathbf{u} = -\mathbf{f}_L(r) \ . \tag{2.11}$$

The only nonvanishing component of the displacement field is in the tangential direction, $\mathbf{u}(\mathbf{r}) = u_\phi(r)\ \hat{\boldsymbol{\phi}}$ and yields a stress $\sigma_{r\phi} = 2c_{66}u_{r\phi}$. For free boundary conditions[23] at the inner and outer circumference of the disk, $[\partial_r\mathbf{u}]_{r=R_1} = [\partial_r\mathbf{u}]_{r=R_2} = 0$, we obtain

$$\sigma_{r\phi}(r) = -\frac{IB_0}{4c\pi t}\left[1 + \frac{1}{r^2}\ln(R_2/R_1)\frac{2R_1^2R_2^2}{R_2^2 - R_1^2}\right] . \tag{2.12}$$

The spatially inhomogeneous stress given by Eq. (2.12) decreases as $1/r^2$ and gives rise to a Peach-Koehler force that can unbind dislocations from bound pairs, yielding free dislocations that in turn contribute to the relaxation of the applied shear.

III. DYNAMICS OF NEUTRAL DISLOCATION PAIRS

Both edge and screw dislocations can occur in the vortex lattice. The geometry and properties of such dislocation lines has been discussed for instance in Ref. 24. For simplicity here we assume that the disk is sufficiently thin that thermally-induced vortex wandering in the direction transverse to the applied field is negligible and the vortices are essentially rigid rods.[25] In this limit, only edge dislocations can occur in the Abrikosov lattice. The dislocation lines are aligned with the z direction and their Burgers vectors lie in the xy plane. The geometry and properties of such rigid dislocation lines are the same as those of point dislocations in two-dimensional lattices. In particular, the bare interaction energy of an isolated pair of dislocations of Burgers vectors $\mathbf{b}^{(1)}$ and $\mathbf{b}^{(2)}$, located at $\mathbf{r}_1$ and $\mathbf{r}_2$, is given by,

$$U_0^B(\mathbf{r}_1-\mathbf{r}_2)=\frac{K_0}{4\pi}\left\{\mathbf{b}^{(1)}\cdot\mathbf{b}^{(2)}\ln\left(\frac{|\mathbf{r}_1-\mathbf{r}_2|}{a_0}\right)-\frac{\mathbf{b}^{(1)}\cdot(\mathbf{r}_1-\mathbf{r}_2)\;\mathbf{b}^{(2)}\cdot(\mathbf{r}_1-\mathbf{r}_2)}{|\mathbf{r}_1-\mathbf{r}_2|^2}\right\} +\frac{E_c t}{a_0^2}\big[|\mathbf{b}^{(1)}|^2+|\mathbf{b}^{(2)}|^2\big], \tag{3.1}$$

where $E_c\sim c_{66}a_0^2$ is the core energy per unit length of an edge dislocation and the coupling constant K_0 is given by

$$K_0=4c_{66}(c_{11}-c_{66})t/c_{11}\approx 4c_{66}t\;. \tag{3.2}$$

The last approximate equality in Eq. (3.2) holds for incompressible lattices. The (dimensionful) Burgers vector $\mathbf{b}$ is defined as the jump in the displacement $\mathbf{u}$ upon integration around a closed contour,

$$\oint d\mathbf{u}=\mathbf{b}\;. \tag{3.3}$$

We are interested here in the nucleation of free dislocations from bound pairs. The interaction energy of a neutral pair, consisting of two dislocations of opposite Burgers vectors, $\mathbf{b}^{(1)}=-\mathbf{b}^{(2)}=-\mathbf{b}$, is

$$U_0^B(\boldsymbol{\rho})=\frac{K_0a_0^2}{4\pi}\left[\ln\left(\frac{|\boldsymbol{\rho}|}{a_0}\right)-\cos^2\theta\right]+2E_ct\;, \tag{3.4}$$

where $\boldsymbol{\rho}=\mathbf{r}_1-\mathbf{r}_2$ and θ is the angle between $\boldsymbol{\rho}$ and $\mathbf{b}$. The quantity $2E_ct$ represents the energy to create a pair of straight edge dislocations of length t at a distance a_0 relative to a dislocation-free system. It plays the role of a chemical potential for dislocation pairs. The strictly two-dimensional limit of point vortices (as opposed to the case of rigid vortex lines considered here) is recovered by the replacement $c_{66}t\to c_{66}^{2d}$, where c_{66} and c_{66}^{2d} are the shear moduli of a three-dimensional and of a two-dimensional lattice, respectively.

In general, many dislocation pairs will be present in the lattice. The interaction of a given pair is then renormalized by a screening cloud of other pairs. Following Kosterlitz and Thouless,[19] this effect can be described in terms of a scale-dependent dielectric constant, $\epsilon(\rho)$. Neglecting the angular part of the dislocation interaction, which is a marginal perturbation at large length scales[26], the effective interaction of a neutral pair is given by

$$U_0(\rho)=\frac{K_0a_0^2}{4\pi}\int_{a_0}^{\rho}\frac{d\rho'}{\epsilon(\rho')\rho'}+2E_ct\;. \tag{3.5}$$

At equilibrium, in the absence of external stresses, the probability per unit area $\Gamma_0(\rho)$ of finding a pair of dislocation of separation ρ is given by

$$\Gamma_0(\rho)=\frac{1}{a_0^4}\exp\Big[-U_0(\rho)/k_BT\Big]\;. \tag{3.6}$$

and remains very small away from the Kosterlitz-Thouless melting transition, $T_M=K_0a_0^2/(16\pi k_B)$. Following Ref. 16, the density of pairs on scales ρ is equivalently defined by the equation,

$$\frac{d\Gamma_0}{d\rho}=-\frac{\overline{K}_0}{\epsilon(\rho)\rho}\Gamma_0(\rho)\;, \tag{3.7}$$

with

$$\overline{K}_0=\frac{K_0a_0^2}{4\pi k_BT} \tag{3.8}$$

a dimensionless coupling constant. Equation (3.7) is naturally rewritten in terms of a scale dependent stiffness, $\overline{K}(\rho)=\overline{K}_0/\epsilon(\rho)$, and a dislocation fugacity, $y(\rho)$, with $[y(\rho)]^2=\rho^4\Gamma_0(\rho)$.[27] The bare fugacity is simply $y_0=y(a_0)=\exp\big[-E_ct/k_BT\big]$. One can then see immediately that Eq. (3.7) is nothing but the first of the Kosterlitz-Thouless recursion relations, usually written in terms of the fugacity as

$$\frac{dy}{d\ln\rho}=\Big[2-\frac{\overline{K}(\rho)}{2}\Big]y\;. \tag{3.9}$$

The scale-dependence of the stiffness arises from the polarization of dislocation pairs and is governed by the second KT recursion relation,

$$\frac{d\overline{K}^{-1}}{d\ln\rho}=2\pi^2y^2\;. \tag{3.10}$$

It is well known that the KT flow equations yield a low-temperature phase with finite long-wavelength dielectric constant, separated by a high-temperature phase where

$\epsilon(\rho) \to \infty$ at large scales and unbound dislocations proliferate. The melting occurs at $\overline{K} = 4$.[19]

To discuss the nonequilibrium nucleation of free dislocations from bound pairs under the action of an applied stress, we need to study the dynamics of neutral dislocation pairs as they move under the action of their mutual interaction and of the Peach-Koehler force due to the external stress field. The position $\mathbf{r}_\nu$ of the Burgers vector $\mathbf{b}^{(\nu)}$ is assumed to obey a Langevin equation of the form,[28]

$$\frac{dr_{\nu i}}{dt} = \mu_{ij}^{(\nu)}\Big[-\sum_{\mu\neq\nu}\frac{\partial U_0(\mathbf{r}_\nu-\mathbf{r}_\mu)}{\partial r_{\nu j}} + F_j^{\mathrm{PK}(\nu)}(\mathbf{r}_\nu)\Big] + \eta_i^{(\nu)}(t)\ , \tag{3.11}$$

where Latin indices denote Cartesian components, $\mu_{ij}^{(\nu)}$ is the mobility tensor, and $\eta_i^{(\nu)}$ is a random white noise, with

$$\langle \eta_i^{(\nu)}(t)\eta_j^{(\mu)}(t')\rangle = 2k_BT\mu_{ij}^{(\nu)}\delta_{\mu\nu}\delta(t-t')\ . \tag{3.12}$$

The force $\mathbf{F}^{\mathrm{PK}(\nu)}$ is the Peach-Koehler force from the external stress and it is given by

$$F_i^{\mathrm{PK}(\nu)}(\mathbf{r}_\nu) = -\epsilon_{ij}\sigma_{jk}(\mathbf{r}_\nu)b_k^{(\nu)}\ . \tag{3.13}$$

Notice that in the case of interest here the external stress is spatially inhomogeneous and the Peach-Koehler force on the n-th Burgers vector is evaluated at the location of the Burgers vector.

As we are interested in the dynamics of a neutral pair, it is convenient to introduce the center of mass and relative coordinates of the pair as

$$\begin{aligned}\boldsymbol{\rho} &= \mathbf{r}_1 - \mathbf{r}_2\ ,\\ \mathbf{R}_{CM} &= \frac{\mathbf{r}_1+\mathbf{r}_2}{2}\ .\end{aligned} \tag{3.14}$$

The Langevin equations for the center of mass and relative coordinates of a single pair are then given by

$$\frac{dR_{CMi}}{dt} = \frac{1}{2}\mu_{ij}\epsilon_{jk}b_l\Big[\sigma_{kl}\big(\mathbf{R}_{CM}+\boldsymbol{\rho}/2\big) - \sigma_{kl}\big(\mathbf{R}_{CM}-\boldsymbol{\rho}/2\big)\Big] + \eta_i^{CM}(t)\ , \tag{3.15}$$

and

$$\frac{d\rho_i}{dt} = \mu_{ij}\epsilon_{jk}b_l\Big[\sigma_{kl}\big(\mathbf{R}_{CM}+\boldsymbol{\rho}/2\big) + \sigma_{kl}\big(\mathbf{R}_{CM}-\boldsymbol{\rho}/2\big)\Big] - 2\mu_{ij}\frac{\partial U_0(\rho)}{\partial\rho_j} + \eta_i(t)\ , \tag{3.16}$$

where $\boldsymbol{\eta} = \boldsymbol{\eta}^{(2)} - \boldsymbol{\eta}^{(1)}$ and $\boldsymbol{\eta}^{CM} = (\boldsymbol{\eta}^{(2)} + \boldsymbol{\eta}^{(1)})/2$. Assuming that all dislocations have the same mobility, i.e., $\mu_{ij}^{(n)} = \mu_{ij}$ for all n, we obtain

$$\langle \eta_i(t)\eta_j(t')\rangle = 2k_BT\mu_{ij}\delta(t-t')\ , \tag{3.17}$$

$$\langle \eta_i^{CM}(t)\eta_j^{CM}(t')\rangle = \frac{k_BT}{2}\mu_{ij}\delta(t-t')\ . \tag{3.18}$$

We now assume that both R_1 and the width of the disk, $R_2 - R_1$, are much larger than a_0, so that the stress field can be considered uniform on the scale a_0 of the initial separation between the dislocations of the pair. We then expand the Peach-Koehler force about its value at the center of mass of the pair. To leading order, we obtain

$$\frac{d\mathbf{R}_{CM}}{dt} \simeq \boldsymbol{\eta}^{CM}(t)\ , \tag{3.19}$$

$$\frac{d\rho_i}{dt} \simeq 2\mu_{ij}\Big[-\frac{\partial U_0(\rho)}{\partial\rho_j} + \epsilon_{jk}\sigma_{kl}(\mathbf{R}_{CM})b_l\Big] + \eta_i(t)\ . \tag{3.20}$$

The center of mass of the pair performs free thermal Brownian motion. We will focus below on the dynamics of the relative coordinate.

The Langevin equation for the relative coordinate can be simplified if we take into account that climb motion is much slower than glide, yielding a strong anisotropy in the diffusion of dislocations. In general the mobility tensor can be written as

$$\mu_{ij} = \mu_{\mathrm{glide}}\hat{b}_i\hat{b}_j + \mu_{\mathrm{climb}}(\delta_{ij} - \hat{b}_i\hat{b}_j)\ , \tag{3.21}$$

where μ_{glide} and μ_{climb} are the mobility associated with the motion of a dislocation in its glide plane (defined by its Burgers vector and $\hat{\mathbf{z}}$) and perpendicular to the glide plane (climb), respectively, and $\hat{\boldsymbol{b}} = \mathbf{b}/a_0$. Since climb can only occur with the creation of vacancies and interstitials, $\mu_{\mathrm{climb}} >> \mu_{\mathrm{glide}}$ [29]. The motion of our edge dislocations is then predominantly unidirectional, along the direction of the Burgers vector. It is convenient to separate the relative displacement of the pair, $\boldsymbol{\rho}$, into its components along the glide and climb directions,

$$\boldsymbol{\rho} = \hat{\mathbf{b}}x + (\hat{\mathbf{z}}\times\hat{\mathbf{b}})y\ , \tag{3.22}$$

where $x = \hat{\mathbf{b}}\cdot\boldsymbol{\rho}$ and $y = (\hat{\mathbf{z}}\times\hat{\mathbf{b}})\cdot\boldsymbol{\rho}$. The Langevin equation for the separation along the glide direction is then given by

$$\frac{dx}{dt} \simeq 2\mu_{\mathrm{glide}}\Big[-\frac{\partial U_0(\rho)}{\partial x} + a_0\sigma_\parallel(\mathbf{R}_{CM})\Big] + \eta_\parallel(t)\ . \tag{3.23}$$

where

$$\sigma_\parallel(\mathbf{R}_{CM}) = \hat{b}_i\epsilon_{ij}\sigma_{jk}(\mathbf{R}_{CM})\hat{b}_k\ , \tag{3.24}$$

and

$$\langle \eta_\parallel(t)\eta_\parallel(t')\rangle = 2k_BT\mu_{\mathrm{glide}}\delta(t-t')\ . \tag{3.25}$$

The Langevin equation for the pair separation can also be written in terms of the total potential energy of the neutral pair in the presence of the external stress as

$$\frac{dx}{dt} = -2\mu_{\rm glide}\frac{\partial U(\rho)}{\partial x} + \eta_{\parallel}(t) \ , \tag{3.26}$$

where

$$U(\rho) = U_0(\rho) + \frac{1}{2}\rho_i\big[\epsilon_{ij}\hat{b}_k + \epsilon_{ik}\hat{b}_j\big]\sigma_{jk}(\mathbf{R}_{CM})t \ . \tag{3.27}$$

For the geometry of interest here the only non-vanishing component of the stress tensor σ_{ij} is $\sigma_{r\phi}$ given in Eq. (2.12). The neutral pairs that can be unbound by this stress when climb is forbidden are those with Burgers vectors along the tangential direction of the disk. Denoting simply by $\mathbf{r}$ the location of the center of mass of the pair relative to the center of the disk and assuming that the separation $\sim a_0$ of the neutral pair is small compared to the width of the disk, the interaction energy of the pair can be written as

$$U(\rho) \approx U_0(\rho) - a_0 x\sigma(r) \ , \tag{3.28}$$

where $\sigma(r) = -\sigma_{r\phi}(r) > 0$ is obtained from Eq.(2.12).

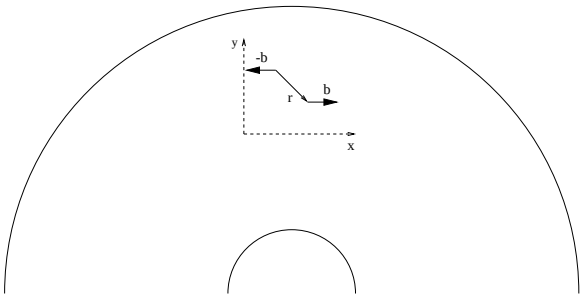

FIG. 2. A pair of dislocations with opposite Burgers vectors. The Burgers vectors are in the tangential direction. The sketch shows the orientation of the pair, but it is not to scale. Also shown is the local coordinate system with axis along the glide and climb directions of the pair used in the text.

A plot of the interaction energy $U(x, y)$ as a function of the separation in the glide direction, x, for finite y is shown in Fig. 3. For simplicity we neglect the angular part of the interaction in zero shear and simply use Eq. (3.5) for U_0. This approximation does not change the qualitative behavior of the results obtained below. For a finite value of the applied stress, the interaction has a saddle point at a location $x_0(y)$ on the positive x axis (for $\sigma_{r\phi} < 0$), defined by $[\partial U/\partial x]_{x=x_0} = 0$ and given by the solution of

$$a_0\sigma\rho_0^2 = x_0\overline{K}(\rho_0)k_BT \ , \tag{3.29}$$

where $\rho_0(y) = \sqrt{x_0^2(y) + y^2}$. For small y,[30]

$$x_0(y) \approx x_c - 2\frac{y^2}{x_c} \ , \tag{3.30}$$

where x_c is the solution of the equation

$$a_0\sigma x_c = \overline{K}(x_c)k_BT \ . \tag{3.31}$$

At low temperatures, where the coupling constant can be replaced by its bare value, we obtain

$$x_c(r) \approx \frac{K_0 a_0}{4\pi\sigma(r)} \ . \tag{3.32}$$

The neutral pair can unbind by escaping over the barrier. This process creates a pair of free dislocations that then contributes to relaxing the applied stress.

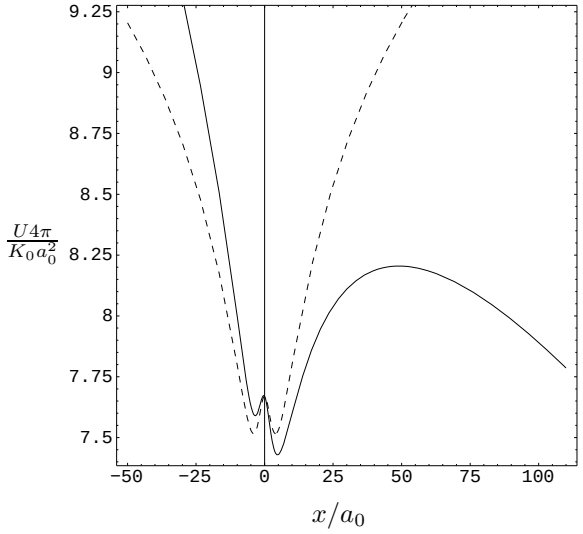

FIG. 3. The interaction energy a neutral dislocation pair in the presence of an applied shear stress as a function of the pair separation along the glide direction, x, for $y = 4a_0$. The value used for the applied stress corresponds to $x_c = 50a_0$. The dashed line shows the interaction energy of the pair for $\sigma = 0$.

At zero temperature the pair can be said to unbind when the saddle point x_0 occurs at a length scale of order a_0. In thick samples, like the one used in the experiments by the Argonne group, this may indeed be the relevant mechanism for unbinding. In thin films on the contrary, we will see that thermal activation plays the dominant role.

To obtain a simple estimate of the critical value of the applied stress where unbinding will occur at zero or very low temperatures, we use the bare value of the pair binding energy and consider a pair with $\theta = 0$, i.e., $y = 0$. The saddle point is then given by Eq. (3.32) and unbinding can be estimated to occur when $x_c(r) \sim a_0$, corresponding to a critical stress

$$\sigma_{cr}^0(r) \approx K_0/(4\pi t) \ . \tag{3.33}$$

This is the simplest "criterion" for the onset of plasticity. By solving for r, one obtains the critical radius $r_{\rm pl}(I)$

where shear induced dislocation unbinding occurs, yielding slippage of neighboring annular sections of the vortex lattice,

$$r_{\rm pl}(I) = \left(\frac{I}{I_0 - I}\right)^{1/2} \sqrt{\frac{2R_1^2 R_2^2}{R_2^2 - R_1^2} \ln\left(\frac{R_2}{R_1}\right)} \ , \qquad (3.34)$$

where $I_0 = cc_{66}t/B_0$ is the current where shear induced proliferation of dislocations occurs across the entire sample.

If we use typical parameters of the experiment by the Argonne group ($R_1 \approx 35\mu m$, $R_2 \approx 350\mu m$, $t \approx 10\mu m$, $H \approx 4T$, and $I \approx 15mA$ in YBCO), we obtain $r_{\rm pl} \approx 100\mu m$. The critical radius $r_{\rm pl}(I)$ which marks the onset of plasticity increases with current, indicating that, since the shear stress is largest near the inner circumference of the disk, "plastic flow" occurs first in annular sections close to the axis. This behavior is qualitatively consistent with the experimental observations. An interesting result of our simple model is that, at high fields, the current scale I_0, and therefore $r_{\rm pl}(I)$, are *independent of the field*.

IV. THERMAL UNBINDING

At finite temperatures, neutral dislocation pairs can unbind by going over the barrier via thermal activation. This is certainly the most relevant mechanism in two dimensions or in thin samples. The theory of stress relaxation via nonlinear unbinding of dislocation pairs was developed some time ago by Ambegaokar and collaborators[13] for superfluid films and by Bruinsma, Halperin, and Zippelius[14] for two-dimensional crystals, and recently applied by Franosch and Nelson[16] to describe nonlinear shear relaxation in smectic liquid crystal films.

Using standard methods, it is convenient to transform the Langevin equation for the pair separation $\boldsymbol{\rho}$ into a Fokker-Planck equation for the density of pairs, $\Gamma(\boldsymbol{\rho})$,[31], given by,

$$\partial_t \Gamma = -\partial_i J_i \ , \qquad (4.1)$$

where

$$J_i = -\mu_{ij}\left[\left(\frac{\partial U_0}{\partial \rho_j} - \epsilon_{jk}\sigma_{kl}(\mathbf{r})b_l\right)\Gamma + k_B T \partial_j \Gamma\right] \qquad (4.2)$$

is the local current of pairs and $\mathbf{r}$ the center of mass of the pair.

Again, we separate the relative displacement $\boldsymbol{\rho}$ in components along the glide and climb directions, as in Eq. (3.22), and neglect climb. Introducing a diffusion constant for glide, $D = \mu_{\rm glide}/k_B T$, and letting $u = U/k_B T$, the Fokker-Planck equation can be written as,

$$\partial_t \Gamma = -\partial_x J_x \ , \qquad (4.3)$$

with

$$\begin{aligned} J_x(x,y) &= -2D[(\partial_x u)\Gamma + \partial_x \Gamma] \qquad (4.4)\\ &= -2De^{-u}\partial_x(e^u \Gamma) \ . \end{aligned}$$

In a steady state, Eq. (4.3) reduces to $\partial_x J_x = 0$ and the current of dislocation pairs (which change their separation in the glide (x) direction) is only a function of the pair separation in the climb (y) direction. It is given by

$$J_x(y) = 2D \ \frac{e^{u(x,y)}\Gamma(x,y)}{\int_x^\infty dx' e^{u(x',y)}} \ , \qquad (4.5)$$

where x is an arbitrary position (with $x >> a_0$, so that the shear stress can be considered uniform). For $x \to \infty$ we expect that the dislocation pair probability density, Γ, vanishes rapidly, yielding

$$J_x(y) \int_x^\infty dx' e^{u(x',y)}) = 2D \ e^{u(x,y)}\Gamma(x,y) \ . \qquad (4.6)$$

The integral on the left hand side of Eq. (4.6) is dominated by the saddle point and the lower limit of integration can therefore be extended to $-\infty$. The integral is evaluated by the method of steepest descent, with the result,

$$\int_x^\infty dx' e^{u(x',y)} \approx \sqrt{\frac{2\pi}{|[\partial_x^2 u(\rho)]_{\rho=\rho_M(y)}|}} e^{u(\rho_M(y))} \ . \qquad (4.7)$$

To evaluate $\Gamma(\rho)$ on the right hand side of Eq. 4.6, we first notice that in the absence of external stress the density Γ will assume its equilibrium form, $\Gamma_0(\rho) = (1/a_0^4)e^{-u_0(\rho)}$. For small stresses and $|x| << x_M$, we assume that a local equilibrium "barometric" form holds, i.e., $\Gamma(x_2,y) = \Gamma(x_1,y)e^{-[u(x_2,y)-u(x_1,y)]}$. The absence of climb implies that the integrated pair density at any y-cross section remains the same before and after the application of stress,

$$\begin{aligned} \int_{-\infty}^{\infty} dx_2 \Gamma_0(x_2,y) &= \int_{-\infty}^{\infty} dx_2 \Gamma(x_2,y) \qquad (4.8)\\ &\approx \int_{-\infty}^{\infty} dx_2 \Gamma(x_1,y) e^{-[u(x_2,y)-u(x_1,y)]} \ . \end{aligned}$$

The main contribution to the integral in the last equality comes from the saddle-point of the full potential $u(x,y)$, while the integral in the first term is dominated by the saddle point $x = 0$ of the potential in the absence of shear stress. After some algebra, we obtain

$$\Gamma(x,y)e^{u(x,y)} \approx \frac{1}{a_0^4}\left[\cosh\left(\frac{a_0 \sigma y}{k_B T}\right)\right]^{-1} \ . \qquad (4.9)$$

Finally, the current is given by,

$$J_x(y) \approx \frac{2D\sqrt{|[\partial_x^2 u(\rho)]_{\rho=\rho_0(y)}|}}{\sqrt{2\pi} a_0^4 \cosh\left(\frac{a_0 \sigma y}{k_B T}\right)} e^{-u(\rho_0(y))} \ . \qquad (4.10)$$

The main approximation used in obtaining this result is that of rare escapes over a high barrier. This requires $\overline{K} >> 1$, which is practically always satisfied as $\overline{K}$ assumes its smallest value, $\overline{K} = 4$, at T_M. We also must have $x_0 >> a_0$, which imposes an upper limit to the value of the external stress.

The dissociation rate of bound dislocation pairs per unit area of the lattice is given by

$$R = \frac{d}{dt}\int_{-\infty}^{+\infty} dy \int_{x_0(y)}^{\infty} dx \Gamma(x,y) = \int_{-\infty}^{+\infty} dy J_x(y) \ . \tag{4.11}$$

To evaluate this integral, we use a saddle-point approximation about $y = 0$, with the result,

$$R \simeq \frac{2D}{x_c^4} y^2(x_c) \frac{e^{\overline{K}(x_c)}}{\sqrt{\overline{K}(x_c)}} \ . \tag{4.12}$$

Dislocations of opposite Burgers vectors recombine when they come within $x_0(y) \approx x_c$ of each other. The net production rate of free dislocations is then given by[13]

$$\frac{\partial n_f}{\partial t} = R - \langle v \rangle x_c n_f^2 \ , \tag{4.13}$$

where n_f is the areal density of free dislocations. The second term on the right hand side of Eq. (4.13) is the recombination rate, with $\langle v \rangle \approx a_0 \sigma D/k_B T$ the mean glide velocity of a free dislocation under the shearing force σa_0 . In the steady state the density of free dislocations is given by $n_f \approx \sqrt{R/(\langle v \rangle x_c)}$, or

$$n_f(T,\sigma) \approx \sqrt{2} \frac{y(x_c)}{x_c^2} \frac{e^{\overline{K}(x_c)/2}}{\left[\overline{K}(x_c)\right]^{3/4}} \ . \tag{4.14}$$

For comparison, the density of free dislocations in equilibrium, in the absence of external stress, is given by

$$n_f^0(T) = \frac{y_0}{a_0^2} = \frac{1}{a_0^2} e^{-E_c t/k_B T} \ . \tag{4.15}$$

The applied shear enhances exponentially $n_f(T,\sigma)$ over its equilibrium value. Equation (4.14) is one of the main results of this section.

To find the explicit dependence of n_f on the applied stress, we need to consider the relative importance of the two length scales entering the problem: the location x_c of the saddle point and the Kosterlitz-Thouless correlation length $\xi_-(T)$, which measures the proximity to the melting transition below T_M. The KT correlation length ξ_- is defined as the length scale above which the scale-dependent interaction $\overline{K}(\rho)$ can be approximated by its large distance limit, $\overline{K}(\rho >> \xi_-) \approx \overline{K}(\rho = \infty) = 4\big[1 + \alpha(T)/4\big]$, with $\alpha(T) \sim (T_M - T)^{1/2}$. It is given by

$$\xi_-(T) = a_0 e^{1/\alpha(T)} \ , \tag{4.16}$$

and diverges as $T \to T_M^-$. In this regime the fugacity is given by $y(\rho >> \xi_-) \approx \alpha(T) \rho^{-\alpha(T)/2}$. If $x_c >> \xi_-$, the coupling constant and the fugacity in Eq. (4.14) can be replaced by their large scale values and the density of free dislocations is given by

$$n_f \sim \overline{\alpha}(T) x_c^{-(2+\alpha(T)/2)} \frac{e^{2(1+\alpha(T)/4)}}{(1+\alpha(T)/4)^{1/4}} \ , \tag{4.17}$$

which yields

$$n_f \sim \sigma^{2+\alpha(T)/2} \ . \tag{4.18}$$

The condition $x_c >> \xi_-$ or $4\pi\sigma/K_0 << e^{-1/\alpha(T)}$ will apply for sufficiently small stress σ, not too close to T_M. As T_M is approached from below, eventually one obtains $\xi_- >> x_c$. In this regime one can approximate[13]

$$\begin{aligned} \overline{K}(x_c) &\approx 4\Big[1 + \frac{1}{2\ln(x_c/a_0)}\Big] \ , \\ y(x_c) &\approx \big[\ln(x_c/a_0)\big]^{-1} \ . \end{aligned} \tag{4.19}$$

The density of free dislocations is then given by

$$n_f \sim \frac{1}{x_c}^2 \big[\ln(x_c/a_0)\big]^{-1} \sim \sigma^2 \ . \tag{4.20}$$

For a Corbino disk of finite thickness t the corresponding Kosterlitz-Thouless transition temperature[32] $T_M = c_{66} t a_0^2/4\pi k_B$ is very large, so that all temperatures of interest are well below T_M . In this region, $\xi_- \sim a_0$ and the coupling constant and the fugacity in Eq. (4.14) can be replaced by their bare values. The density of free dislocations induced by the external stress is given by

$$n_f(T,\sigma) \approx n_f^0(T) \frac{a_0^2}{x_c^2} \frac{e^{\overline{K}_0/2}}{\overline{K}_0^{3/4}} \ \sim \ \sigma^2 \ . \tag{4.21}$$

At a finite temperature below T_M we can define a condition for "shear-induced melting" as the value of the external stress where $x_c(\sigma) \simeq \xi_-(T)$. Notice that for $T << T_M$, this condition reduces to the one used at $T = 0$ to obtain Eq. (3.33). By solving this for σ as a function of T, we find that near T_M the critical shear stress $\sigma_c(r)$ where unbound dislocations proliferate in the vortex lattice is given by

$$\sigma_c(r) \sim \frac{K_0}{4\pi} e^{-b/(T_M - T)^{1/2}} \ , \tag{4.22}$$

with $b > 0$ a numerical constant. The temperature dependence of this simple estimate is consistent with the experimental observation by the Argonne group that the applied stress (which is determined by the driving current) required for the onset of plasticity decreases with increasing temperature (see Fig. 4 of Ref. 10). By combining the various estimates for the critical shear stress where unbound dislocations proliferate, i.e. the vortex lattice is "shear-melted", we obtain the schematic phase diagram shown in Fig. 4.

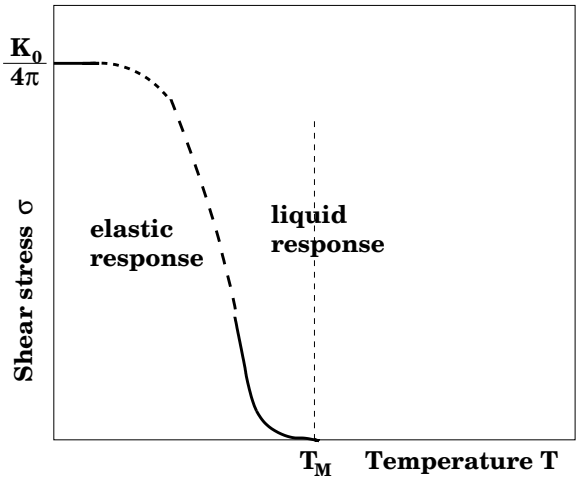

FIG. 4. A schematic phase diagram in the (σ, T) plane. The dashed vertical line is the location of the Kosterlitz-Thouless melting temperature T_M where thermal unbinding of neutral pairs occurs in the absence of external shear. At a finite shear stress, free dislocations proliferate at the lower temperature denoted by the thick continuous-dashed line. Even at $T = 0$ a finite shear stress $\sim K_0/4\pi$ is sufficient to free bound pairs. The dashed portion of the line separating the regions where neutral pairs are bound and the vortex lattice responds elastically from the region where free dislocations proliferate and the vortex arrays flows plastically is an interpolation (by eye) between the low and high $(T \to T_M^-)$ estimates obtained in the text.

Finally, recalling that in the Corbino disk geometry the external stress has the spatially inhomogeneous form given in Eq. (2.12), we can solve Eq. (4.22) for the critical radius $r_{\rm pl}(I,T)$ where shear-melting first takes place for a given value of applied current and temperature. We find that Eq. (3.34) for the critical radius at $T = 0$ generalizes simply to finite temperatures as $r_{\rm pl}(I,T)$ is obtained from Eq. (3.34) by the replacement $I_0 \to I_0(T) = I_0 \exp\big[-b/(T_M - T)^{1/2}\big]$.

In the region below T_M and above $\sigma_c(r)$, the driven vortex array can be described as a lattice with a concentration $n_f(\sigma(r), T)$ of unbound dislocations, moving at a steady rate along the direction of their Burgers vectors. Moving dislocations relax a strain. This provides a mechanism for nonlinear stress relaxation that naturally yields nonlinear IV characteristics in the superconductor.

Assuming that the annular width of the disk is much larger than a_0, so that a hydrodynamic description can be used, we define a Burgers-vector density,

$$\boldsymbol{\mathcal{B}}(\mathbf{r}, t) = \sum_\nu \hat{\boldsymbol{b}}^{(\nu)} \delta(\mathbf{r} - \mathbf{r}_\nu) \ , \tag{4.23}$$

which is related to the local strain in the lattice by

$$\epsilon_{ik}\partial_k w_{ij} = a_0 \mathcal{B}_j \ , \tag{4.24}$$

where w_{ij} is the unsymmetrized strain tensor. It is related to the displacement field by $w_{ij} = \partial_i u_j$. In the presence of unbound dislocations, the displacement field is no longer single-valued, as indicated in Eq. (3.3), and local deformations of the medium are more conveniently described in terms of the local strain w_{ij}. Since free dislocations are always created in pairs, the Burgers-vector density is conserved,

$$\partial_t \mathcal{B}_i + \partial_j \mathcal{J}^i_j = 0 \ , \tag{4.25}$$

where $\mathcal{J}^i_j$ is the current of the i-th component of Burgers-vector density in the j-th direction, namely

$$\mathcal{J}^i_j = \sum_\nu \hat{b}^{(\nu)}_i \frac{dr_{\nu j}}{dt} \delta(\mathbf{r} - \mathbf{r}_\nu) \ . \tag{4.26}$$

The equation for the displacement field is replaced by an equation for the local strain, given by

$$\partial_t w_{ij} = \frac{1}{n_0}\partial_i j_j + a_0 \epsilon_{ik} \mathcal{J}^j_k \ , \tag{4.27}$$

where $\mathbf{j} = n_0 \mathbf{v}$ (to linear order) is the number current density, with $\mathbf{v}$ the local velocity of the vortex array.

In the Corbino disk geometry of interest here, the only nonvanishing component of the dislocation current is in the azimuthal direction. Combining Eq. (4.27) (specialized to a steady state) with the results obtained in section IV, we estimate,

$$\partial_r v_\phi(r) = -a_0 J^\phi_\phi \sim [\sigma(r)]^{1+\overline{K}(x_c)/2} \ , \tag{4.28}$$

where we have used Eq. (4.10) evaluated at $y = 0$ to obtain the dependence of the dislocation current on the shear stress. The dependence on shear rate is highly nonlinear as $x_c \sim 1/\sigma(r)$. The field from flux motion is radial and its magnitude is

$$E(r) = \frac{1}{c} B_0 v_\phi(r) \ . \tag{4.29}$$

The net voltage drop across the disk is given by

$$\Delta V = \int_{R_1}^{R_2} E(r) dr \sim \int_{R_1}^{R_2} dr \int_{R_1}^{r} dr' [\sigma(r')]^{1+\overline{K}(x_c)/2} \ . \tag{4.30}$$

If $x_c >> \xi_-(T)$, we can replace $\overline{K}$ by its asymptotic value. Since $\sigma(r) \sim I$, this immediately gives a nonlinear dependence $\Delta V \sim I^{3+\alpha/8}$. The exponent α is nonuniversal, with $\alpha \sim (T_M - T)^{1/2}$.

V. DISCUSSION

We have presented a theoretical analysis of recent transport experiments on vortex lattices in the Corbino disk geometry. In the experiments, the onset of plasticity corresponds to the onset of nonlinearity in the IV

characteristics and an unconventional scaling of the voltage with radial distance from the center of the disk.[9–11] The nonlinear voltage-current scaling is found to be $\Delta V \sim I^{3+\alpha(T)/8}$, with α a nonuniversal exponent that depends on temperature.

In our theoretical model, the onset of plasticity is associated with the proliferation of free dislocations which break away from tightly bound pairs. In general, two mechanisms can be responsible for the nucleation of free dislocations from bound pairs: an externally applied shear stress and thermal fluctuations. In the absence of external shear, the thermally induced proliferation of free dislocations is simply the Kosterlitz-Thouless melting transition of the lattice. A finite shear stress as the one imposed on the vortex lattice by the external current in the Corbino experiment can unbind dislocations below the KT transition temperature and even at $T = 0$. Using standard methods of stochastic dynamics, we have calculated the density of free dislocations as a function of applied stress and the temperature. In contrast to earlier work on nonlinear shear relaxation in superfluid,[13] solid[15,14] and smectic[16] films, here the external stress is spatially inhomogeneous. As a result, proliferation of unbound dislocations occurs for different values of the external current at different locations in the disk.

The mechanism for the onset of plasticity proposed here, namely the proliferation of free dislocations, is certainly relevant for thin Corbino disks, where the vortex lattice is essentially two-dimensional. In order to compare our results with the experiments we have assumed that even in a Corbino disk of finite thickness dislocations are essentially rigid over the thickness of the sample — in other words screw dislocations are excluded. In this case, the problem becomes essentially two-dimensional. The energy cost for creating a dislocation pair is, however, proportional to the sample thickness. This raises considerably the barrier that bound pairs have to overcome to unbind via thermal activation. The finite temperature calculation may therefore only be relevant in very thin samples, while in thick disks the physics is captured by the simple $T = 0$ estimate described in Section 3. Both at zero and finite temperature, our results, however, agree qualitatively with the experimental observations, indicating that a simple picture of stress-induced dislocation unbinding can account for the spatial dependence of the onset of plasticity. Specifically, we find that (1) "shear-induced melting" starts at the inner boundary and propagates towards the outer rim of the disk as the driving current is increased, (2) the "critical" current for the onset of plastic slip of concentric vortex lattice planes decreases with increasing temperature, and (3) the calculated critical radius where plastic slip occurs for a fixed current is of the same order of magnitude as the value measured in experiments.

A direction for future work is the study of the role of dislocation climb, which will of course require to couple dislocation dynamics to that of vacancies and interstitials. In addition, it would clearly be very interesting to consider dislocation dynamics in the presence of quenched disorder.

This work was supported by the National Science Foundation through grant DMR-9805818.

---

[1] G. W. Crabtree and D. R. Nelson, Phys. Today **50(4)**, 38 (1997).

[2] G. Blatter *et al.*, Rev. Mod. Phys. **66**, 1125 (1994).

[3] D. R. Nelson, in *Phenomenology and Applications of High-Temperature Superconductors* (Addison Wesley, Reading, Massachusetts, 1992), p. 187.

[4] D. S. Fisher, M. P. A. Fisher, and D. Huse, Phys. Rev. B **43**, 130 (1991).

[5] D. R. Nelson and V. N. Vinokur, Phys. Rev. B **48**, 13 060 (1993).

[6] M. C. Marchetti and D. R. Nelson, Phys. Rev. B **42**, 9938 (1990).

[7] D. A. Huse and S. N. Majumdar, Phys. Rev. Lett. **71**, 2473 (1993).

[8] M. C. Marchetti and D. R. Nelson, Physica C **330**, 105 (2000) (e-print: arXiv:cond-mat/9909382).

[9] D. López *et al.*, Phys. Rev. Lett. **82**, 1277 (1999).

[10] G. W. Crabtree *et al.*, J. Low Temp. Phys. **117**, 1313 (1999).

[11] G. W. Crabtree *et al.*, Physica C **341-348**, 995 (2000).

[12] M. C. Marchetti, Physica C **341-348**, 991 (2000) (e-print: arXiv:cond-mat/0007467).

[13] V. Ambegaokar, B. I. Halperin, D. R. Nelson, and E. D. Siggia, Phys. Rev. B **21**, 1806 (1980).

[14] R. Bruinsma, B. I. Halperin, and A. Zippelius, Phys. Rev. B **25**, 579 (1982).

[15] A. Zippelius, B. I. Halperin, and D. R. Nelson, Phys. Rev. B **22**, 2514 (1980).

[16] T. Franosch and D. R. Nelson, Phys. Rev. E **63**, 61706 (2001) (e-print: arXiv:cond-mat/0012433).

[17] A.Pertsinidis and X. S. Ling, Phys. Rev. Lett. **87**, 98303 (2001) (e-print: arXiv:cond-mat/0012306).

[18] A. Pertsinidis and X. S. Ling, (e-print: arXiv:cond-mat/0103293).

[19] See, e.g., D. R. Nelson, in *Phase Transitions and Critical Phenomena*, Vol. 7, edited by C. Domb and J. Lebowitz (Academic, London, 1983) pp. 76-79.

[20] Y. Paltiel *et al.*, Phys. Rev. Lett. **85**, 3712 (2000) (e-print: arXiv:cond-mat/0008092).

[21] F. Haenssler and L. Rinderer, Helv. Phys. Acta **40**, 659 (1967).

[22] M. C. Marchetti and D. R. Nelson, Physica C **174**, 40 (1991).

[23] No-slip boundary conditions for the displacement yield a stress of the form given in Eq. (2.12), but with the plus sign inside the square bracket replaced by a minus sign. In this case the stress is largest (in magnitude) at the inner and outer rims of the disk and vanishes in the interior.

Plastic slip will occur first at the rims, and then propagate towards the interior of the disk as the current is increased. No-slip boundary conditions are relevant for the experimental geometry proposed in Ref. 8 of a Corbino disk with Bose glass contacts.

[24] M. C. Marchetti and D. R. Nelson, Phys. Rev. B **41**, 1910 (1990).

[25] M. C. Miguel and M. Kardar, Phys. Rev. B **56**, 11 903 (1997) (e-print: arXiv:cond-mat/9706161).

[26] D. R. Nelson, Phys. Rev. B **18**, 2318 (1978).

[27] The same symbol y is used here for the fugacity and below for the separation of a neutral pair of dislocations along the climb direction. There should be no confusion as he meaning of y will be clear from the context.

[28] We have neglected the force arising from Peierls barriers to glide motion due to the periodicity of the lattice. In the Langevin equation for the separation of the dislocation pair in the glide direction considered below, this force only couples to gradients of the external stress.

[29] F. R. N. Nabarro and A. T. Quintanilha, in *Dislocations in Solids* (North-Holland Pub. Co., Amsterdam, 1980), Vol. 5.

[30] Taking into account the angular part of the dislocation interaction only changes the numerical coefficient of the y^2 term in the expression for the saddle point.

[31] S. Chandrasekhar, Rev. Mod. Phys. **15**, 58 (1943).

[32] D. R. Nelson and J. M. Kosterlitz, Phys. Rev. Lett. **39**, 1201 (1977).